Vol 16 No 11, November 2007
1009-1963/2007/16(11)/3407-09

Chinese Physics

© 2007 Chin. Phys. Soc.
and IOP Publishing Ltd

Six-wave mixing phase-dispersion by optical heterodyne detection in dressed reverse N-type four-level system*

Gan Chen-Li(甘琛利)[a)b)], Nie Zhi-Qiang (聂志强)[a)], Li Ling(李 岭)[a)], Shen Lei-Jian(沈磊剑)[a)], Zhang Yan-Peng(张彦鹏)[a)b)†], Song Jian-Ping(宋建平)[a)], Li Yuan-Yuan(李院院)[a)], Zhang Xiang-Chen(张相臣)[a)], and Lu Ke-Qing(卢克清)[c)]

[a)] *Key Laboratory for Physical Electronics and Devices of the Ministry of Education, Xi'an Jiaotong University, Xi'an* 710049, *China*
[b)] *Department of Physics, University of Arkansas, Fayetteville, Arkansas* 72701, *USA*
[c)] *State Key Laboratory of Transient Optics and Technology, Xi'an Institute of Optics and Precision Mechanics, Chinese Academy of Sciences, Xi'an* 710068, *China*

(Received 10 December 2006; revised manuscript received 28 March 2007)

We have investigated the dressed effects of non-degenerate four-wave mixing (NDFWM) and demonstrated a phase-sensitive method of studying the fifth-order nonlinear susceptibility due to atomic coherence in RN-type four-level system. In the presence of a strong coupling field, NDFWM spectrum exhibits Autler–Townes splitting, accompanied by either suppression or enhancement of the NDFWM signal, which is directly related to the competition between the absorption and dispersion contributions. The heterodyne-detected nonlinear absorption and dispersion of six-wave mixing signal in the RN-type system show that the hybrid radiation-matter detuning damping oscillation is in the THz range and can be controlled and modified through the colour-locked correlation of twin noisy fields.

Keywords: four-wave mixing, six-wave mixing
PACC: 4250, 4265, 3280

1. Introduction

Four-wave mixing (FWM) and six-wave mixing (SWM) are the third-order and fifth-order nonlinear optical processes, respectively, in which the input beams induce a nonlinear polarization in a medium, giving rise to the generation of a coherent beam. The FWM signal is directly related to the third-order nonlinear susceptibility $\chi^{(3)}$, which exhibits resonant characteristic of the medium, thus FWM with resonant excitations can be employed as a versatile spectroscopic technique. Similarly, SWM is corresponding to the fifth-order nonlinear susceptibility $\chi^{(5)}$ and it can also be used as a tool to study the nonlinearity of the researched medium. For example, in degenerate four-wave mixing (DFWM), the three input beams and the signal beam have an identical frequency. When the frequency is such as to cause the signal to be in resonance with a molecule the signal will be enhanced tremendously as a result of multiple resonant terms. Based on this feature, the DFWM has been developed as a diagnostic method of detecting trace molecule species in combustion environments. The DFWM is also shown to be able to serve as a means of probing rotational anisotropy in nonequilibrium ensembles of gaseous molecules.

In recent years, people have been interested in using the resonance-enhanced non-degenerate four-wave mixing (NDFWM) as a new tool for various purposes and it does work well and manifests some advantages, such as free choice of interaction volume, excellent spatial signal resolution and simple optical alignment compared with the DFWM. For example, we have used it to study the vibrational dephasing in molecular materials both in the frequency-domain and in the time-domain. We have proposed a kind

*Project supported by the National Natural Science Foundation of China (Grant Nos 60308002 and 60678005), the Foundation for the Author of National Excellent Doctoral Dissertation of China (Grant No 200339), the Research Foundation from Ministry of Education of China (Grant No 105156), the For Ying-Tong Education Foundation for Young Teachers of Higher Education Institutions of China (Grant No 101061) and the Specialized Research Fund for the Doctoral Program of Higher Education of China (Grant No 20050698017).
†Corresponding author. E-mail: ypzhang@mail.xjtu.edu.cn

of Doppler-free laser spectroscopy, which we called ultra-fast modulation spectroscopy,[1−5] to measure the energy levels of an atomic system. This technique is based on the interference between macroscopic polarizations that are excited simultaneously in the medium. In addition, a Rayleigh-enhanced NDFWM,[4,5] which can be employed for the measurement of ultra-fast longitudinal relaxation time in the frequency-domain, was demonstrated recently. This technique can be applied even to an absorbing medium if a time-delayed method, which is based on the field-correlation effects, is adopted.[4−6]

Our previous studies on the NDFWM and SWM were restricted to two- or three-photon resonance in two- or three-level systems. In this paper we study two-photon resonant NDFWM and three-photon SWM in dressed atomic systems. Specifically, we consider an RN-type four-level system in which the two upper levels are coupled by a strong laser field. This scheme involves resonant three-photon excitation, therefore highly excited atomic states can be studied with high sensitivity. We find that in the presence of the coupling field the two-photon resonant NDFWM signal can be suppressed or enhanced due to the quantum interference. Using this method, not only the resonant frequency and transverse relaxation rate but also the dipole moment of the transition can be deduced.

In this paper, we presented a novel type of phase-sensitive detection for the fifth-order complex susceptibility in a multi-level gas medium. We study three-photon SWM in sub- femtosecond polarization beats induced by the fifth-order susceptibility. In our heterodyne detection scheme, the reference signal is the two-photon resonant NDFWM signal, which is induced by the ω_1 frequency component in beam 1 and ω_2 in beam 2 and 3. The SWM signal beam and the NDFWM reference beam then interfere directly at the detector. Our method is based on femtosecond polarization interference between NDFWM and SWM processes in a pure homogeneously-broadened or Doppler-broadened three-level ladder-type system[3−5] and it is a good and easy way to measure the fifth-order susceptibility, by which way we measure the real and imaginary parts of the susceptibility directly. The modified third-order absorption and dispersion can be controlled coherently by noisy light colour-locking bandwidth, frequency detuning, and time delay. The Doppler-free counter-propagation configuration we use allows us to observe these interesting nonlinear effects in a long atomic vapour cell.

This paper is organized as follows. Section 2 presents the Autler–Townes splitting in the NFWM spectrum and its numerical derivation. We show that in the presence of a strong coupling field, the NFWM spectrum splits into two separate peaks, which is known as AT splitting. The coupling field can also lead to either suppression or enhancement of the NFWM signal. Section 3 presents the numerical results and the theory of our phase-sensitive heterodyne detection. Finally, Section 4 gives the discussion and conclusion. We point out that the two-photon resonant NDFWM signal in dressed atoms provides an effective spectroscopic tool of measuring not only the resonant frequency and dephasing rate but also the transition dipole moment between two highly excited atomic states, and we also demonstrate that the phase-sensitive heterodyne detection method is good way to study the nonlinear effects under various limits and conditions.

2. Autler–Townes splitting in the NDFWM spectrum

We first consider two-photon resonant NDFWM in a Λ-type three-level system [Figs.1(a) and 1(b)], where states between $|0\rangle$ and $|1\rangle$ and between $|1\rangle$ and $|2\rangle$ are coupled by dipolar transitions with resonant frequencies denoted by Ω_1 and Ω_2 and dipole moment matrix elements μ_1 and μ_2, respectively. As shown in Fig.1(a), beams 2 and 3 have the same frequency ω_2 and a small angle exists between them; beam 1 with frequency ω_1 propagates along the opposite direction of beam 2. The ω_1 and ω_2 will connect the transition from $|0\rangle$ to $|1\rangle$ and $|1\rangle$ to $|2\rangle$, respectively. The simultaneous interactions of atoms with beams 1 and 2 will induce atomic coherence between $|0\rangle$ and $|2\rangle$ through two-photon excitation. This coherence is probed by beam 3, and as a result a NDFWM signal (beam 4) of frequency ω_1 is generated in the direction almost opposite to the direction of beam 3. Next when ω_3 and $-\omega_3$ are turned on [Fig.1(c)], the coherence between $|0\rangle$ and $|3\rangle$ is excited, and as a result a three-photon resonant SWM signal of frequency ω_1 is generated (beam 4).

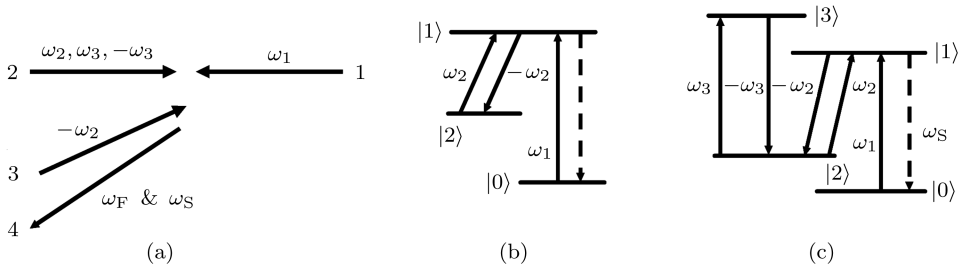


Fig.1. Schematics of NDFWM and SWM (a), energy-level diagram for two-photon resonant NDFWM (b), and energy-level diagram for three-photon SWM (c).

The stochastic fields of beam 2 ($E_{\rm p2}$), beam 3 ($E_{\rm p3}$) and beam 1 (E_1) are expressed as

$$E_{\rm p2} = \varepsilon_2 u_2(t)\exp[{\rm i}(\boldsymbol{k}_2\cdot\boldsymbol{r}-\omega_2 t)] + \varepsilon_3 u_3(t)\exp[{\rm i}(\boldsymbol{k}_3\cdot\boldsymbol{r}-\omega_3 t)] + \varepsilon_3' u_3(t-\tau)\exp[{\rm i}(\boldsymbol{k}_3'\cdot\boldsymbol{r}-\omega_3 t+\omega_3\tau)], \quad (1)$$

$$E_{\rm p3} = \varepsilon_2' u_2(t-\tau)\exp[{\rm i}(\boldsymbol{k}_2'\cdot\boldsymbol{r}-\omega_2 t+\omega_2\tau)] \ \text{ and } \ E_1 = A_1(\boldsymbol{r},t)\exp(-{\rm i}\omega_1 t) = \varepsilon_1 u_1(t)\exp[{\rm i}(\boldsymbol{k}_1\cdot\boldsymbol{r}-\omega_1 t)]. \quad (2)$$

Here, ε_i, $\boldsymbol{k}_i(\varepsilon_i'$, $\boldsymbol{k}_i')$ are the constant field amplitude and the wave vector of the ω_i component; $u_i(t)$ is a dimensionless statistical factor that contains phase and amplitude fluctuations; τ is a relative time delay between the prompt (unprime) and delayed (prime) fields. Beam 1 is assumed to be a quasi-monochromatic light ($u_1(t)\approx 1$). To accomplish this arrangement the frequency components of ω_2 and ω_3 lights are split and then recombined to provide one and three frequency pulses in such a way that the ω_2 component is delayed by τ in beam 3 and the ω_3 component delayed by the same amount in beam 2 (Fig.1(a)).

We assume the common detuning to be $\Delta_1 = \Omega_1-\omega_1$, $\Delta_2 = \Omega_2-\omega_2$ and $\Delta_3 = \Omega_3-\omega_3$. Since the nonlinear polarizations responsible for the two-photon resonant NDFWM and three-photon SWM signal are proportional to the off-diagonal density matrix elements $\rho_{10}^{(3)}$ and $\rho_{10}^{(5)}$ respectively, which can be obtained from the density matrix equations with relaxation terms properly included, we can directly obtain them by the perturbation chains using the density matrix dynamic equations. The perturbation chains that are corresponding to the NDFWM and SWM processes are as follows:

$$\text{(I)}\quad \rho_{00} \xrightarrow{\omega_1} \rho_{10} \xrightarrow{-\omega_2} \rho_{20} \xrightarrow{\omega_2} \rho_{10}, \quad (3)$$

$$\text{(II)}\quad \rho_{00} \xrightarrow{\omega_1} \rho_{10} \xrightarrow{-\omega_2} \rho_{20} \xrightarrow{\omega_3} \rho_{30} \xrightarrow{-\omega_3} \rho_{20} \xrightarrow{\omega_2} \rho_{10}. \quad (4)$$

The Liouville pathway can also be clearly described by double-sided Feynman diagrams (DSFDs) shown in Fig.2. Using the density matrix dynamic equations, we obtain

$$\frac{\partial\hat{\rho}(t)}{\partial t} = \frac{1}{{\rm i}\hbar}[\hat{H}_0+\hat{H}_1(t),\hat{\rho}(t)] - \Gamma\hat{\rho}. \quad (5)$$

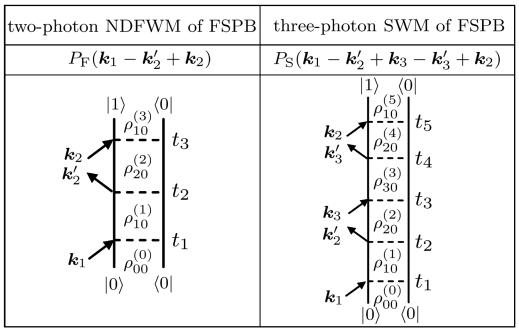


Fig.2. The double-sided Feynman diagrams of FWM and SWM Liouville pathway.

By solving the density matrix dynamic equations and using partially rotating wave approximation we obtain the density matrix expression and its approximation under assumption $|G_3|^2 \ll \Gamma_{20}\Gamma_{30}$ as below:

$$\rho_{10}^{(3)} = \frac{-{\rm i}G_1G_2G_2'^{*}{\rm e}^{{\rm i}(\boldsymbol{k}_1+\boldsymbol{k}_2-\boldsymbol{k}_2')\cdot\boldsymbol{r}}[\Gamma_{30}+{\rm i}(\Delta_1-\Delta_2+\Delta_3)]}{(\Gamma_{10}+{\rm i}\Delta_1)^2\{[\Gamma_{20}+{\rm i}(\Delta_1-\Delta_2)][\Gamma_{30}+{\rm i}(\Delta_1-\Delta_2+\Delta_3)]+|G_3|^2\}}, \quad (6)$$

$$\rho_{10}^{(3)} \approx \frac{-{\rm i}(G_2')^{*}G_1G_2\exp[{\rm i}(\boldsymbol{k}_1+\boldsymbol{k}_2-\boldsymbol{k}_2')\cdot\boldsymbol{r}]}{(\Gamma_{10}+{\rm i}\Delta_1)^2[\Gamma_{20}+{\rm i}(\Delta_1-\Delta_2)]}\times\left\{1-\frac{|G_3|^2}{[\Gamma_{20}+{\rm i}(\Delta_1-\Delta_2)][\Gamma_{30}+{\rm i}(\Delta_1-\Delta_2+\Delta_3)]}\right\}. \quad (7)$$

Here, we define the coupling coefficients $G_1 = \mu_1\varepsilon_1/\hbar$, $G_2 = \mu_2\varepsilon_2/\hbar$ and $G_2' = \mu_2\varepsilon_2'/\hbar$, the transverse relaxation rate Γ_{n0} between states $|n\rangle$ and $|0\rangle$, and we assume that ε_1, ε and ε_2' are weak so that the perturbation theory is applicable and the atoms are initially in the ground state $|0\rangle$, i.e. $\rho_{00}^{(0)} = 1$. The NDFWM signal intensity is proportional to the $\left|\rho_{10}^{(3)}\right|^2$. The two-photon NDFWM results above is a form of Doppler-free spectrum when the incident lasers have narrow bandwidths. On the basis of two-photon NDFWM in the Λ-type three-level system, we use an additional coupling field of frequency $\omega_3(\approx \Omega_3)$ to drive the transition from $|2\rangle$ to $|3\rangle$ so as to induce atomic coherence between states $|0\rangle$ and $|3\rangle$. In the same way, we assume that ε_1, ε_2 and ε_2' are weak whereas the coupling field ε_3 has an arbitrary magnitude, and we can obtain the fifth-order nonlinear susceptibility expression as below:

$$\rho_{10}^{(5)} = \frac{\mathrm{i}G_1G_2(G_2')^*\left|G_3\right|^2\exp[\mathrm{i}(\boldsymbol{k}_1+\boldsymbol{k}_2-\boldsymbol{k}_2'+\boldsymbol{k}_3-\boldsymbol{k}_3)\cdot\boldsymbol{r}]}{(\Gamma_{10}+\mathrm{i}\Delta_1)^2[\Gamma_{20}+\mathrm{i}(\Delta_1-\Delta_2)]^2[\Gamma_{30}+\mathrm{i}(\Delta_1-\Delta_2+\Delta_3)]}. \tag{8}$$

Therefore, we can see from expression (7) that the third-order susceptibility under the weak field approximation is the sum of the result of FWM and the result of SWM; the first term on the right-hand side corresponds to the two-photon resonant NDFWM. The second term corresponds to the three-photon resonant SWM, as shown by Eqs.(6) and (8). Figure 3 presents the NDFWM signal intensity versus $(\Delta_1 - \Delta_2)/\Gamma_{30}$. The maximum of the signal intensity with $G_3/\Gamma_{30} = 0$ is normalized to 1. We can find that as the strong coupling field G_3 is increased a dip appears at the line centre first, and then the spectrum splits into two separate peaks. This is AT splitting, which reflects the levels of the dressed states. The two peaks are located symmetrically with respect to $\Delta_1 - \Delta_2 = 0$ when the coupling field is exactly in resonance (Fig.3(a)). On the other hand, for the case of $\Delta_3 \neq 0$ the two separate peaks become asymmetric, which is more evident for small values of G_3/Γ_{30} (Fig.3(b)).

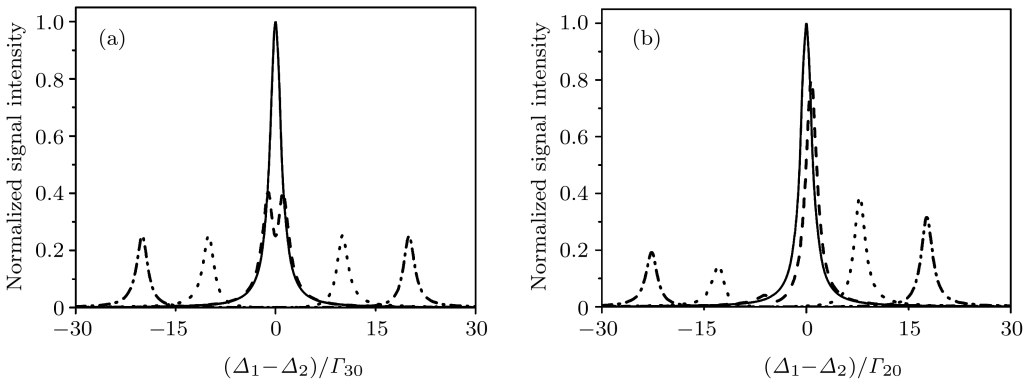


Fig.3. NDFWM signal intensity versus $(\Delta_1 - \Delta_2)/\Gamma_{30}$ for (a) $\Delta_3 = 0$, $\Gamma_{10}/\Gamma_{30} = 1$, $\Gamma_{20}/\Gamma_{30} = 1$, $G_3/\Gamma_{10} = 0$ (solid curve), $G_3/\Gamma_{30} = 1$(dashed curve), $G_3/\Gamma_{30} = 10$ (dotted curve) and $G_3/\Gamma_{30} = 20$ (dash-dotted curve), respectively; (b) $\Delta_3/\Gamma_{30} = 10$, $\Gamma_{10}/\Gamma_{30} = 1$, $\Gamma_{20}/\Gamma_{30} = 1$, $G_3/\Gamma_{30} = 0$ (solid curve), 1 (dashed curve), 10 (dotted curve) and 20 (dash-dotted curve). The maximum of NDFWM signal intensity with G_3/Γ_{30} is normalized to 1.

Now, we study the AT splitting in the NDFWM spectrum. For simplicity, we consider the case where the coupling field is in resonance $\Delta_3 = 0$. According to expression (6), the signal intensity, which is proportional to $\left|\rho_{10}^{(3)}\right|^2$, is given by

$$I(\Delta) \propto \frac{\Delta^2 + \Gamma_{30}^2}{\Delta^4 + (\Gamma^2 - 2g^2)\Delta^2 + g^4}. \tag{9}$$

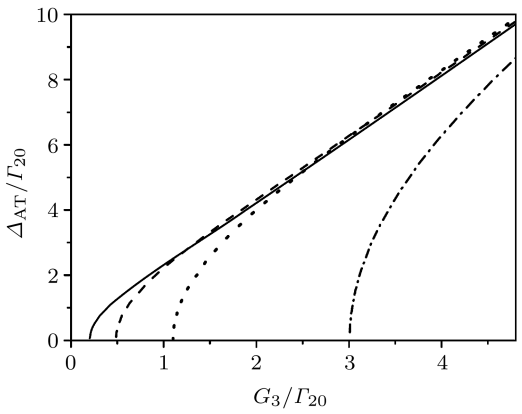


Fig.4. AT splitting of NDFWM $\Delta_{\rm AT}/\Gamma_{20}$ versus G_3/Γ_{20} for $\Gamma_{30}/\Gamma_{20}=0.5$ (solid curve), $\Gamma_{30}/\Gamma_{20}=1$ (dashed curve), $\Gamma_{30}/\Gamma_{20}=2$ (dotted curve), $\Gamma_{30}/\Gamma_{20}=5$ (dash-dotted curve).

Here, $\Delta=\Delta_1-\Delta_2$, $\Gamma=\Gamma_{20}+\Gamma_{30}$ and $g^2=G_3^2+\Gamma_{20}\Gamma_{30}$. The condition for the appearance of peaks is $\mathrm{d}I(\Delta)/\mathrm{d}\Delta=0$, which leads to

$$\Delta^4+2\Gamma_{30}^2\Delta^2+(\Gamma_{30}^2\Gamma^2-2\Gamma_{30}^2g^2-g^4)=0. \quad (10)$$

We thus obtain $\Delta^2=G_3[G_3^2+2\Gamma_{30}(\Gamma_{20}+\Gamma_{30})]^{1/2}-\Gamma_{30}^2$ and the AT splitting is given as

$$\Delta_{\rm AT}=2\{G_3[G_3^2+2\Gamma_{30}(\Gamma_{20}+\Gamma_{30})]^{1/2}-\Gamma_{30}^2\}^{1/2}. \quad (11)$$

Figure 4 gives the G_3-dependence of the AT splitting. In the limit of $G_3\ll\Gamma_{20}\Gamma_{30}$, we can obtain $\Delta_{\rm AT}=2G_3$ from expression (11).

3. Dispersion and absorption of the SWM and its heterodyne detection

In this section, we presents the FWM and SWM results in another way, i.e. by taking into consideration the fluctuations of both amplitude and phase, which is given by the statistical factor $u_i(t)$, just as their heterodyne detection results given by expressions (1) and (2). Now, we use the two perturbation chains (3) and (4) and the density matrix dynamic equations to obtain the polarization results as below:

$$\begin{aligned}P_{\rm F}(\boldsymbol{v},t)&=N\mu_1\int_{-\infty}^{+\infty}\mathrm{d}\boldsymbol{v}w(\boldsymbol{v})\rho_{10}^{(3)}(\boldsymbol{v})\\&=S_1(\boldsymbol{r})\exp[-\mathrm{i}(\omega_1t+\omega_2\tau)]\int_{-\infty}^{+\infty}\mathrm{d}\boldsymbol{v}w(\boldsymbol{v})\int_0^{\infty}\mathrm{d}t_3\int_0^{\infty}\mathrm{d}t_2\int_0^{\infty}\mathrm{d}t_1\\&\quad\times\exp[-\mathrm{i}\theta^{(\rm I)}]H_1(t_1)H_2(t_2)H_1(t_3)u_2^*(t-t_2-t_3-\tau)u_2(t-t_3), \quad (12)\\P_{\rm S}(\boldsymbol{v},t)&=N\mu_1\int_{-\infty}^{+\infty}\mathrm{d}\boldsymbol{v}w(\boldsymbol{v})\rho_{10}^{(5)}(\boldsymbol{v})\\&=S_2(\boldsymbol{r})\exp\{-\mathrm{i}[\omega_1t+(\omega_2+\omega_3)\tau]\}\int_{-\infty}^{+\infty}\mathrm{d}\boldsymbol{v}w(\boldsymbol{v})\int_0^{\infty}\mathrm{d}t_5\int_0^{\infty}\mathrm{d}t_4\int_0^{\infty}\mathrm{d}t_3\int_0^{\infty}\mathrm{d}t_2\int_0^{\infty}\mathrm{d}t_1\exp[-\mathrm{i}\theta^{(\rm II)}]\\&\quad\times H_1(t_1)H_2(t_2)H_3(t_3)H_2(t_4)H_1(t_5)u_2(t-t_5)u_3^*(t-t_4-t_5-\tau)u_3(t-t_3-t_4-t_5)\\&\quad\times u_2^*(t-t_2-t_3-t_4-t_5-\tau), \quad (13)\end{aligned}$$

where, $H_1(t)=\mathrm{e}^{-d_1t}$, $H_2(t)=\mathrm{e}^{-d_2t}$, $H_3(t)=\mathrm{e}^{-d_3t}$; $A=S_1(\boldsymbol{r})\mathrm{e}^{-\mathrm{i}(\omega_1t+\omega_2\tau)}$, $B=S_2(\boldsymbol{r})\mathrm{e}^{-\mathrm{i}(\omega_1t+\omega_2\tau+\omega_3\tau)}$; $S_1(\boldsymbol{r})=-\mathrm{i}N\mu_1^2\mu_2^2\varepsilon_1\varepsilon_2(\varepsilon_2')^*\mathrm{e}^{\mathrm{i}\boldsymbol{k}_{\rm f}\cdot\boldsymbol{r}}/\hbar^3$, $S_2(\boldsymbol{r})=\mathrm{i}N\mu_1^2\mu_2^2\mu_3^2\varepsilon_1\varepsilon_2(\varepsilon_3')^*\varepsilon_3(\varepsilon_2')^*\mathrm{e}^{\mathrm{i}\boldsymbol{k}_{\rm s}\cdot\boldsymbol{r}}/\hbar^5$; $d_1=\Gamma_{10}+\mathrm{i}\Delta_1$, $d_2=\Gamma_{20}+\mathrm{i}\Delta_a$, $d_2'=\Gamma_{20}-\mathrm{i}\Delta_a$, $d_3=\Gamma_{30}+\mathrm{i}\Delta_b$, $\Delta_a=\Delta_1-\Delta_2$ and $\Delta_b=\Delta_1-\Delta_2+\Delta_3$; $\theta^{(\rm I)}(\boldsymbol{v})=\boldsymbol{v}\cdot[\boldsymbol{k}_1(t_1+t_2+t_3)+\boldsymbol{k}_2(t_2+t_3)-\boldsymbol{k}_2't_3]$, $\theta^{(\rm II)}(\boldsymbol{v})=\boldsymbol{v}\cdot[\boldsymbol{k}_1(t_1+t_2+t_3+t_4+t_5)+\boldsymbol{k}_2(t_2+t_3+t_4+t_5)-\boldsymbol{k}_3'(t_3+t_4+t_5)+k_3(t_4+t_5)-\boldsymbol{k}_2't_5]$. The nonlinear polarizations $P_{\rm F}$ and $P_{\rm S}$ correspond to FWM and SWM respectively. In the expression $w(v)$ is the velocity distribution function. The physical processes of FWM and SWM we have discussed in our previous work [4,5] and we do not give them in detail here. For simplicity, here we neglect the Doppler effects, which is mathematically expressed as the approximation $k_iv\approx0$ and $k_i'v\approx0$. Thus after performing the tedious integration we obtain the polarization results below. In a purely homodyne broaden medium when the time delay $\tau>0$ the polarization results becomes

$$P_{\rm F} = \frac{A\exp[-\alpha_2\tau]}{d_1^2(d_2+\alpha_2)}, \tag{14}$$

$$P_{\rm S} = \frac{B\exp[-\alpha_2\tau]}{d_1^2(\alpha_2+d_2)^2}\left[\frac{{\rm e}^{-\alpha_3\tau}-{\rm e}^{-(\alpha_2+d_3)\tau}}{\alpha_2-\alpha_3+d_3} + \frac{{\rm e}^{-(\alpha_2+d_3)\tau}}{\alpha_2+\alpha_3+d_3}\right]. \tag{15}$$

Using the relationship between the susceptibility and polarizations we can obtain the third- and fifth-order susceptibilities as below:

$$\begin{aligned}\chi_{\rm F} &= \frac{P_1}{\varepsilon_0 < E_2(E_2')^* > E_1} \\ &= -\frac{{\rm i}N\mu_1^2\mu_2^2}{\varepsilon_0\hbar^3}\frac{1}{d_1^2(d_2+\alpha_2)}, \\ \chi_{\rm S} &= \frac{P_2}{\varepsilon_0 < E_3^{'*}E_3E_2^{'*}E_2 > E_1} \\ &= \frac{{\rm i}N\mu_1^2\mu_2^2\mu_3^2}{\varepsilon_0\hbar^5}\frac{{\rm e}^{\alpha_3\tau}}{d_1^2(\alpha_2+d_2)^2}\left[\frac{{\rm e}^{-\alpha_3\tau}-{\rm e}^{-(\alpha_2+d_3)\tau}}{\alpha_2-\alpha_3+d_3}\right.\end{aligned} \tag{16}$$

$$\left. + \frac{{\rm e}^{-(\alpha_2+d_3)\tau}}{\alpha_2+\alpha_3+d_3}\right]. \tag{17}$$

We can see from expression (17) that the fifth-order susceptibility contains the radiation-matter oscillation, which is known as radiation-matter detuning oscillation (RDO), and it shows that both atom and light response together. We can also see that the nonlinear susceptibility strongly depends on the time-delay τ and linewidth α_i, and it can be modified by the colour-locked noisy fields. The real and imaginary parts of $\chi_{\rm B}$ correspond to the modified dispersion and absorption of the fifth-order susceptibility. For the absorption curves, the positive value indicates gain and the anomalous dispersion generally corresponds to strong absorption of the medium. Figures 5(a) and 5(b) present the dispersion and absorption of the fifth-order susceptibility with obvious RDO and Figure 5(e) gives their RDO frequency values.

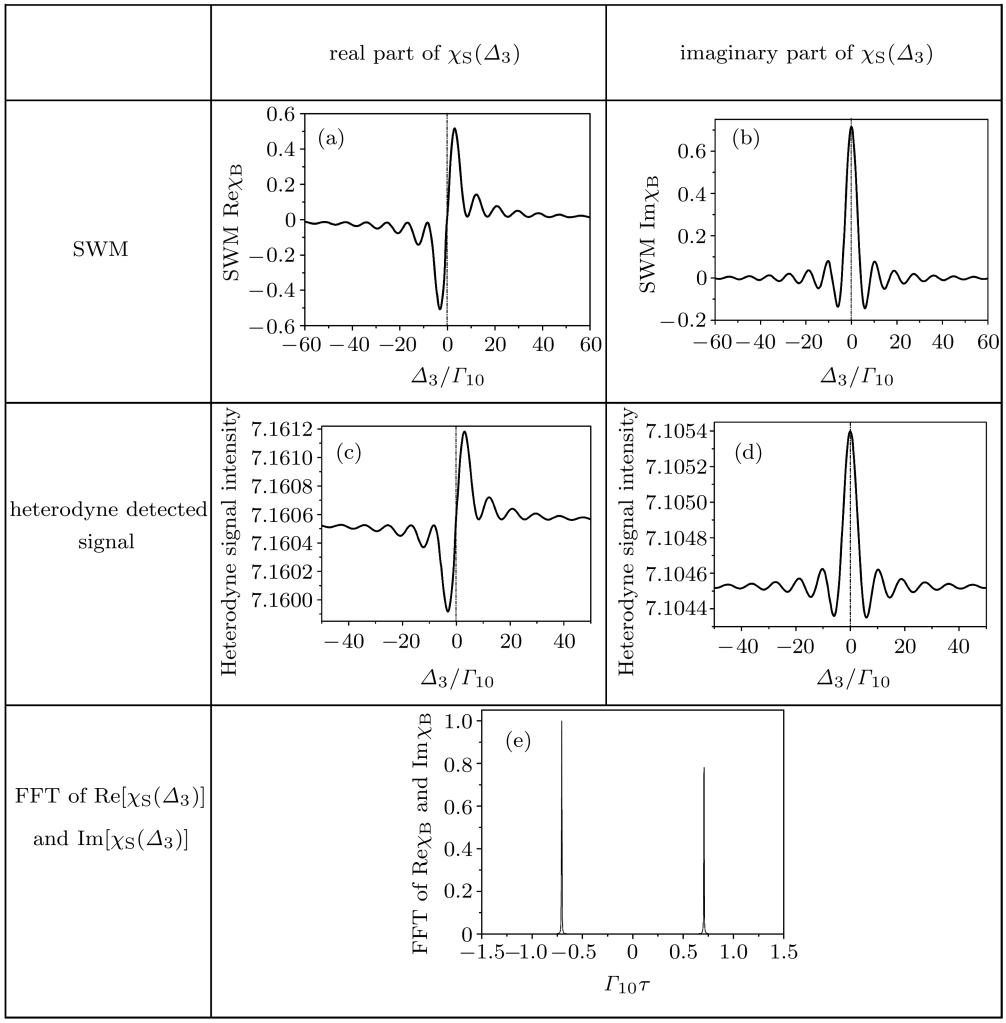


Fig.5. The nonlinear dispersion and absorption of SWM and their heterodyne detection results (for $\tau > 0$) versus Δ_3/Γ_{10} with $\alpha_2/\Gamma_{10} = \alpha_3/\Gamma_{10} = 10$, $\Delta_1/\Gamma_{10} = 0.01$, $\Delta_2/\Gamma_{10} = 0.01$, $\Gamma_{10}\tau = 0.705685$ (dispersion) and $\Gamma_{10}\tau = 0.706078$ (absorption). FFT stands for fast Fourier transform.

Now, we introduce a phase-sensitive detection to detect the real and imaginary parts of SWM, which is known as heterodyne detection. Our heterodyne detection is based on the polarization interference between the FWM and SWM processes at the detector. Since the optical fields oscillate too quickly to detect directly, we have to introduce the FWM polarization $P_{\rm F}$, which is designed in frequency and wave vector so as to conjugate it in its complex representation with the SWM polarization $P_{\rm S}$. Thus, the femtosecond polarization beat (FSPB) signal intensity can be obtained as follows:

$$I(\tau,\Delta_i,\alpha_i)\propto \mathrm{e}^{-2\alpha_2\tau}[|\chi_{\rm F}|^2+\eta_0^2|\chi_{\rm S}|^2\mathrm{e}^{-2\alpha_3\tau} +2\eta_0|\chi_{\rm F}||\chi_{\rm S}|\mathrm{e}^{-\alpha_3\tau}\cos(\theta_{\rm F}-\theta_{\rm S}+\theta)]. \tag{18}$$

Here $\chi_{\rm F}=|\chi_{\rm F}|\mathrm{e}^{\mathrm{i}\theta_{\rm F}}=|\chi_{\rm F}|\cos\theta_{\rm F}+\mathrm{i}|\chi_{\rm F}|\sin\theta_{\rm F}$, $\chi_{\rm S}=|\chi_{\rm S}|\mathrm{e}^{\mathrm{i}\theta_{\rm S}}=|\chi_{\rm S}|\cos\theta_{\rm S}+\mathrm{i}|\chi_{\rm S}|\sin\theta_{\rm S}$, $\theta_{\rm R}=\omega_3\tau-\Delta\boldsymbol{k}\cdot\boldsymbol{r}$, $\Delta\boldsymbol{k}=(\boldsymbol{k}_3-\boldsymbol{k}_3')$, $\eta_0=(\varepsilon_3')^*\varepsilon_3$.

Although the complex susceptibilities (nonlinear responses) are greatly modified by the colour-locked noisy fields, they can still be obtained effectively in an ideal limit. Expression (18) corresponds to the homodyne signal intensity, while in the heterodyne detection, we assume that $|P_{\rm F}|^2\gg|P_{\rm S}|^2$ at intensity level ($|\chi_{\rm F}|\gg|\chi_{\rm S}|$ at field level), so the reference signal (NDFWM) originating from the ω_2 frequency components of the twin beams 2 and 3 is much larger than the SWM signal originating from the frequency components ω_2 and ω_3 of the twin beams 2 and 3. After the approximation, we can obtain the heterodyne signal intensity

$$I(\tau,\Delta_i,\alpha_i)\propto \mathrm{e}^{-2\alpha_2\tau}[|\chi_{\rm F}|^2+2\eta_0|\chi_{\rm F}||\chi_{\rm S}| \times\mathrm{e}^{-\alpha_3\tau}\cos(\theta_{\rm F}-\theta_S+\theta)]. \tag{19}$$

Expression (19) indicates that the FSPB signal of heterodyne detection is modulated with the frequency ω_3 as τ is varied. The phase coherent control of the light beams in FSPB is subtle. Such an FSPB can effectively be employed via optical heterodyne detection to yield the real and imaginary parts of $\chi_{\rm F}$. If we adjust the time delay τ and $\boldsymbol{r}$ such that $\theta_{\rm F}+\theta_{\rm R}=2n\pi$ (i.e. $\tau=[\theta_{\rm F}(\tau)+\Delta\boldsymbol{k}\cdot\boldsymbol{r}-2n\pi]/\omega_3$, $\Delta\boldsymbol{k}\cdot\boldsymbol{r}=0$, the value of integer n depends on the sign of τ sensitively), then

$$I(\Delta_3)\propto \mathrm{e}^{-2\alpha_2\tau}[|\chi_{\rm F}|^2+2\eta_0|\chi_{\rm F}| \times\mathrm{e}^{-\alpha_3\tau}\mathrm{Re}[\chi_{\rm S}(\Delta_3)]. \tag{20}$$

However, if $\theta_{\rm F}+\theta_{\rm R}=(2n+1/2)\pi$ (i.e. $\tau=[\theta_{\rm F}(\tau)+\Delta\boldsymbol{k}\cdot\boldsymbol{r}-2n\pi-\pi/2]/\omega_3$, $\Delta\boldsymbol{k}\cdot\boldsymbol{r}=0$), we have

$$I(\Delta_3)\propto \mathrm{e}^{-2\alpha_2\tau}[|\chi_{\rm F}|^2+2\eta_0|\chi_{\rm F}| \times\mathrm{e}^{-\alpha_3\tau}\mathrm{Im}[\chi_{\rm S}(\Delta_3)]. \tag{21}$$

By changing the time delay τ between beams 2 and 3 we can obtain the real and imaginary parts of $\chi_{\rm S}(\Delta_3)$. The subtle value of τ is generally determined by the gradually approaching method from $\theta_{\rm F}(\tau)+\theta_{\rm R}(\tau)=2n\pi$ or $(2n+1/2)\pi$. Due to the local oscillator intensity that is brought about by the reference signal, the dispersion and absorption only show positive values compared with Figs.5(a) and 5(b). After subtracting the local oscillator background from them, they then turn to being in good agreement with Figs.5(a) and 5(b). This method can only be used for detecting SWM for it has the unique detuning Δ_3 compared with NDFWM. Figures 5(c) and 5(d) give the heterodyne detection results which obviously reflect the real and imaginary parts of $\chi_{\rm S}(\Delta_3)$. Figure 5(e) gives the RDO frequency values of $\mathrm{Re}[\chi_{\rm S}(\Delta_3)]$ and $\mathrm{Im}[\chi_{\rm S}(\Delta_3)]$. When the time delay $\tau<0$, we can also obtain the integration results of the FWM and SWM polarizations that correspond to expressions (12) and (13)

$$P_{\rm F}=\frac{A}{d_1^2}\left(\frac{\mathrm{e}^{\alpha_2\tau}-\mathrm{e}^{d_2\tau}}{d_2-\alpha_2}+\frac{\mathrm{e}^{d_2\tau}}{d_2+\alpha_2}\right), \tag{22}$$

$$\begin{aligned}P^{(\mathrm{II})}=&\frac{B\mathrm{e}^{\alpha_3\tau}}{d_1^2(\alpha_3+d_3-d_2)}\left\{\frac{(\alpha_2+\alpha_3+d_3)[\mathrm{e}^{d_2\tau}-\mathrm{e}^{(\alpha_3+d_3)\tau}]+(\alpha_3+d_3-d_2)\mathrm{e}^{d_3\tau}}{(\alpha_2+d_2)^2(\alpha_2+\alpha_3+d_3)}\right.\\&+\frac{\mathrm{e}^{(\alpha_3+d_3)\tau}-[1+(\alpha_3+d_3-d_2)\tau]\mathrm{e}^{d_2\tau}}{(\alpha_2+d_2)(\alpha_3+d_3-d_2)}\\&+\frac{(\alpha_3-\alpha_2+d_3)[1+(\alpha_2-d_2)\tau][\mathrm{e}^{(\alpha_3+d_3)\tau}-\mathrm{e}^{d_2\tau}]+(\alpha_3+d_3-d_2)[\mathrm{e}^{\alpha_2\tau}-\mathrm{e}^{(\alpha_3+d_3)\tau}]}{(\alpha_2-d_2)^2(\alpha_2-\alpha_3+d_3)}\\&\left.+\frac{(\mathrm{e}^{(\alpha_3+d_3)\tau}-\mathrm{e}^{d_2\tau})[1-(\alpha_3+d_3-d_2)\tau]}{(\alpha_2-d_2)(\alpha_3+d_3-d_2)}\right\}.\end{aligned} \tag{23}$$

Then using the relationship between the susceptibility and polarization we can obtain the third- and fifth-order susceptibilities as below:

$$\chi_{\rm F} = -\frac{{\rm i}N\mu_1^2\mu_2^2}{\hbar^3}\frac{{\rm e}^{-\alpha_2\tau}}{d_1^2}\left(\frac{{\rm e}^{\alpha_2\tau}-{\rm e}^{d_2\tau}}{d_2-\alpha_2}+\frac{{\rm e}^{d_2\tau}}{d_2+\alpha_2}\right), \tag{24}$$

$$\begin{aligned}\chi_{\rm S} = {} & \frac{{\rm i}N\mu_1^2\mu_2^2\mu_3^2}{\hbar^5}\frac{{\rm e}^{-\alpha_2\tau}}{d_1^2(\alpha_3+d_3-d_2)}\left\{\frac{(\alpha_2+\alpha_3+d_3)[{\rm e}^{d_2\tau}-{\rm e}^{(\alpha_3+d_3)\tau}]+(\alpha_3+d_3-d_2){\rm e}^{d_3\tau}}{(\alpha_2+d_2)^2(\alpha_2+\alpha_3+d_3)}\right.\\ & +\frac{{\rm e}^{(\alpha_3+d_3)\tau}-[1+(\alpha_3+d_3-d_2)\tau]{\rm e}^{d_2\tau}}{(\alpha_2+d_2)(\alpha_3+d_3-d_2)}\\ & +\frac{(\alpha_3-\alpha_2+d_3)[1+(\alpha_2-d_2)\tau][{\rm e}^{(\alpha_3+d_3)\tau}-{\rm e}^{d_2\tau}]+(\alpha_3+d_3-d_2)[{\rm e}^{\alpha_2\tau}-{\rm e}^{(\alpha_3+d_3)\tau}]}{(\alpha_2-d_2)^2(\alpha_2-\alpha_3+d_3)}\\ & \left.+\frac{({\rm e}^{(\alpha_3+d_3)\tau}-{\rm e}^{d_2\tau})[1-(\alpha_3+d_3-d_2)\tau]}{(\alpha_2-d_2)(\alpha_3+d_3-d_2)}\right\}.\end{aligned} \tag{25}$$

We can see from expressions (24) and (25) that the third- and fifth-order susceptibilities are greatly modified by the colour-locked noisy fields and if the laser linewidth is much larger than the relaxation rate ($\alpha_i \gg \Gamma_{i0}$), the nonlinear susceptibility strongly depends on the linewidth α_i and the time delay τ. In the purely homogeneously broadened medium, we can use the same way as that in the case of $\tau > 0$ to obtain the real and imaginary parts of $\chi_{\rm S}(\Delta_3)$ and thus obtain their dispersion and absorption curves. Since the fifth-order susceptibility contains the radiation-matter detuning oscillation terms, which are corresponding to the response to both light and atoms, we can see clearly the RDO phenomenon at the tails of the dispersion and absorption curves. Figures 6(a) and 6(b) give the dispersion and absorption curves that are corresponding to the real and imaginary parts of $\chi_{\rm S}(\Delta_3)$. Since our detection is based on the interference between the FWM and SWM at the detector, the homodyne signal intensity can be viewed as the sum of three contributions, i.e. the NDFWM signal intensity ($|P_{\rm F}|^2$), the SWM signal intensity ($|P_{\rm S}|^2$) and cross term between NDFWM and SWM ($P_{\rm F}^* P_{\rm S} + P_{\rm F} P_{\rm S}^*$). If we use nonlinear susceptibility to replace the polarization, we have the homodyne detected signal intensity as follows:

$$\begin{aligned}I(\tau,\Delta_{\rm i},\alpha_{\rm i}) \propto {} & {\rm e}^{2\alpha_2\tau}[|\chi_{\rm F}|^2+\eta_0^2|\chi_{\rm S}|^2{\rm e}^{2\alpha_3\tau}\\ & +2\eta_0|\chi_{\rm F}||\chi_{\rm S}|\\ & \times{\rm e}^{\alpha_3\tau}\cos(\theta_{\rm F}-\theta_{\rm S}+\theta)].\end{aligned} \tag{26}$$

The equation above gives us the homodyne-detected signal intensity when time delay $\tau < 0$ while time delay $\tau > 0$, the signal intensity is given by expression (18). Expressions (18) and (26) contain rich dynamics of the colour-locked noisy-field correlation effects,[6] and the competition between femtosecond modulation and hybrid RDO. Close inspection of expressions (18) and (26) reveals some interesting points: (a) change frequency ω_3, the femtosecond oscillation within RDO will be thicker; (b) when the detuning Δ_2/Γ_{10} decreases, the RDO oscillation period will decrease; (c) the frequency can be read in Table 1, which is the combination of $\Gamma_{10}\tau > 0$ and $\Gamma_{10}\tau < 0$. Figure 6 presents the homodyne detection results and its RDO frequency components. In order to observe the FSPB more clearly, the solid curve has been multiplied by 2000, while dashed line by 1000 and dotted curve by 5000.

Table 1. Ultrafast oscillation frequencies and RDO frequencies of the FSPB signal intensity between NDFWM and SWM under Doppler-free limit.

FSPB between NDFWM and SWM			
time delay	$\tau > 0$	$\tau < 0$	combination of $\tau > 0$ and $\tau < 0$
Doppler free	$(\Delta_1-\Delta_2+\Delta_3)$, ω_3, $\omega_3+(\Delta_1-\Delta_2+\Delta_3)$	$(\Delta_1-\Delta_2)$, $(\Delta_1-\Delta_2+\Delta_3)$, Δ_3, ω_3, $\omega_3-(\Delta_1-\Delta_2)$, $\omega_3-(\Delta_1-\Delta_2+\Delta_3)$, $\omega_3+(\Delta_1-\Delta_2)$, $\omega_3-\Delta_3$	$(\Delta_1-\Delta_2)$, $(\Delta_1-\Delta_2+\Delta_3)$, Δ_3, ω_3, $\omega_3-(\Delta_1-\Delta_2)$, $\omega_3-(\Delta_1-\Delta_2+\Delta_3)$, $\omega_3+(\Delta_1-\Delta_2)$, $\omega_3-\Delta_3$, $\omega_3+(\Delta_1-\Delta_2+\Delta_3)$

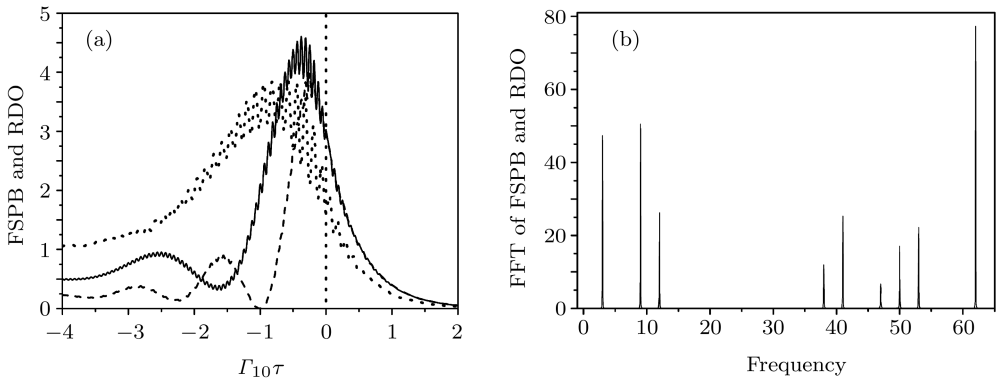


Fig.6. The femtosecond polarization beat, RDO and its FFT in the Doppler free medium. (a) FSPB and RDO versus $\Gamma_{10}\tau$. $\alpha_2/\Gamma_{10}=1$, $\alpha_3/\Gamma_{10}=1$, $\Delta_1/\Gamma_{10}=5$, $\Delta_2/\Gamma_{10}=2$, $\Delta_3/\Gamma_{10}=9$, $\omega_3=100$ (solid curve); $\Delta_2/\Gamma_{10}=0.1$ (dashed curve); $\Delta_1/\Gamma_{10}=0.5$, $\omega_3=50$ (dotted curve); (b) FFT of FSPB and RDO. The frequencies from left to right correspond to $\Delta_1-\Delta_2$, Δ_3, $\Delta_1-\Delta_2+\Delta_3$, $\omega_3-(\Delta_1-\Delta_2+\Delta_3)$, $\omega_3-\Delta_3$, $\omega_3-(\Delta_1-\Delta_2)$, ω_3, $\omega_3+(\Delta_1-\Delta_2)$, $\omega_3+(\Delta_1-\Delta_2+\Delta_3)$.

4. Discussion and conclusion

Two-photon NDFWM is a good tool for spectroscopic analysis, and in the presence of a strong coupling field NDFWM exhibits Autler–Townes splitting, accompanied by either suppression or enhancement of the NDFWM. This also provides us a new way to investigate the slow light effects.[7−9] NDFWM can also be employed to measure the fifth-order susceptibility directly. Using NDFWM as a reference signal, we can easily measure the real and imaginary parts of $\chi_S(\Delta_3)$, which is known as heterodyne detection.

As a time-domain technique, the main advantage of heterodyne detection over the conventional quantum beat is that the temporal resolution is not limited by the laser pulse and the phase information of susceptibility can be retained. Since the heterodyne-detected signal intensity is proportional to real and imaginary parts of susceptibility, we can take a full measure of the complex susceptibility, including its phase. The method presented here is simple to employ and can be applied to a large variety of materials.

In summary, we have demonstrated a phase-sensitive heterodyne method to study the SWM in a Reverse-N-type four-level atomic system. The reference signal is NDFWM signal, which propagates somewhat differently from the SWM signal. This point is very important since the reference signal always travels in basically the same direction; such that it is much easier to match modes and reduce background. This method can also be used to investigate the phase dispersion of the fifth-order susceptibility and the optical heterodyne detection of the three-photon SWM signal under various limits and conditions.

References

[1] DeBeer D, Usadi E and Hartmann S R 1988 *Phys. Rev. Lett.* **60** 1262

[2] Ma H and de Araujo C B 1993 *Phys. Rev. Lett.* **71** 3649

[3] Sun J, Zuo Z C, Mi X, Yu Z H, Wu L A and Fu P M 2005 *Acta Phys. Sin.* **54** 149 (in Chinese)

[4] Zhang Y P, Gan C L, Li L, Ma R Q, Song J P, Jiang T, Yu X J, Li C S, Ge H and Lu K Q 2005 *Phys. Rev.* A **72** 013812
Zhang Y P, Gan C L and Xiao M 2006 *Phys. Rev.* A **73** 053801

[5] Zhang Y P, de Araujo C B and Eyler E E 2001 *Phys. Rev.* A **63** 043802
Zhang Y P, Gan C L, Song J P, Yu X J, Ma R Q, Ge H, Li C S and Lu K Q 2005 *Phys. Rev.* A **71** 023802

[6] Ulness D J 2003 *J. Phys. Chem.* A **107** 8111

[7] Harris S E 1997 *Phys. Today* **50**(7) 36

[8] Li Y and Xiao M 1996 *Opt. Lett.* **21** 1064

[9] Wu Y 2005 *Phys. Rev.* A **71** 053820
Wu Y and Deng L 2004 *Opt. Lett.* **29** 1144
Wu H B, Chang H, Ma J, Xie C D and Wang H 2005 *Acta Phys. Sin.* **54** 8 (in Chinese)